7-18-2006

Shape-Persistent Macrocyclic Aromatic Tetrasulfonamides: Molecules with Nanosized Cavities and their Nanotubular Assemblies in Solid State

Lan He
Beijing Normal University

Yu An
Beijing Normal University

Lihua Yuan
State University of New York at Buffalo

Wen Feng
State University of New York at Buffalo

Minfeng Li
Colleges of Chemistry and Resources Science and Technology, Beijing Normal University, Beijing 100875, China

See next page for additional authors

Published in *Proceedings of the National Academy of Sciences of the United States of America* 103:29 (July 18, 2006), pp. 10850-10855. doi: 10.1073/pnas.0602912103

Submitted April 10, 2006; accepted May 26, 2006; published online July 10, 2006. Edited for PNAS by Jack Halpern, University of Chicago

Shape-persistent macrocyclic aromatic tetrasulfonamides: Molecules with nanosized cavities and their nanotubular assemblies in solid state

Lan He,[1] Yu An,[1] Lihua Yuan,[2] Wen Feng,[2] Minfeng Li,[2] Dechun Zhang,[1] Kazuhiro Yamato,[2] Chong Zheng,[3] Xiao Cheng Zeng,[4] and Bing Gong[1,2]

[1] Colleges of Chemistry and Resources Science and Technology, Beijing Normal University, Beijing 100875, China
[2] Department of Chemistry, University at Buffalo, State University of New York, Buffalo, NY 14260
[3] Department of Chemistry, Northern Illinois University, DeKalb, IL 60115
[4] Department of Chemistry, University of Nebraska, Lincoln, NE 68588
Corresponding authors — L. He helan1961@hotmail.com or B. Gong bgong@chem.buffalo.edu

Abstract: Alkoxy side-chain-flanked diarylsulfonamide serves as a reliable structural motif for constructing macrocyclic aromatic tetrasulfonamides. This 90° structural motif is persistent both in solution and in the solid state, which allows the one-step formation of tetrasulfonamide macrocycles. These macrocycles adopt a cone-shaped conformation in solution and in the solid state. For each molecule, an interior cavity surrounded by the aromatic residues is formed. The cavity sizes of the macrocycles can be tuned by incorporating aromatic residues of proper sizes. Guest (solvent) molecules are found in the cavities and bound by side chains. In solution, ^{1}H NMR shows that the cone conformations undergo rapid interconversion at room temperature. The alkoxy side chains are found to be indispensable for maintaining the cone conformation. In addition, these porous molecules self-assemble into hollow tubular structures in the solid state. A variety of host molecules and building blocks for constructing nanoporous solid-state structures can be expected from these molecules.

Keywords: macrocycle, nanocavity, nanotube, oligomer, sulfonamide

Macrocyclic molecules have served as the basis for designing various receptors of organic molecules (1) and as building blocks for constructing nanoporous structures (2–4). Of particular interest are cavity-containing molecules such as calixarenes (5–12) and cyclodextrins (13). One common feature shared by many macrocycles is their multiple, dynamic conformations (7, 10, 11). For example, among the four different conformations of the well studied calix[4]arenes, the cone conformation leads to an internal cavity for hosting neutral guest molecules of complementary sizes. The conformations of larger calixarenes are even more complicated because of increased flexibility (14). As a result, various strategies to limit the conformational freedom of calixarenes have been reported. It was found that calixarenes with rigid cavities could not only serve as hosts that bind guest molecules with enhanced specificity and strength (15–18) but also provide scaffolds for the presentation of chemical functionality, which lead to efficient catalysts and precise control of intermolecular assemblies (19). Covalent modification of resorcinarenes has also led to rigid, deep cavitands that completely encapsulate sizable molecules (20).

Over the last several years, we have developed folded helical oligomers based on a backbone-rigidification strategy (21, 22). In a recent attempt to design folded aromatic oligosulfonamides, we discovered cyclic aromatic tetrasulfonamides **1a-b**, which adopt a cone conformation reminiscent of that of calix[4]arenes in the solid state (23). Results from two-dimensional (2D) NMR (NOESY) studies suggested that such a cone conformation also prevailed in solution. The cavity of these macrocycles was found to accommodate small solvent molecules such as *N*,*N*′-dimethylformamide (DMF). These newly discovered macrocycles raised several interesting questions as follows. (*i*) Can the observed cone conformation be extended to the creation of analogous cone-shaped molecules of different sizes? (*ii*) How dynamic is the cone conformation in solution? (*iii*) Are the ether side chains flanking the sulfonamide groups necessary for the adoption of the cone conformation?

In this work, we describe that the diarylsulfonamide moiety flanked by phenolic ether side chains, which can be viewed as the basic structural motif of **1a-b** (see Structure 1), adopts a well defined conformation that is predisposed to forming four-residue, macrocyclic sulfonamides. By incorporating naphthalene residues, cone-shaped macrocycles with a cavity larger than that of **1a-b** were obtained in one step. The enlarged cavity was found to host guest molecules such as pyridine in the solid state. Although evidence from both x-ray crystallography and 2D NMR indicated that the cone conformation was persistent both in the solid phase and in solution, variable-temperature NMR indicated that such a conformation was highly dynamic, undergoing rapid inversion between cone conformations. *Ab initio* calculations were carried out on a cone conformation and its partially inverted conformations. Removing some of the ether side chains leads to a macrocycle adopting a 1,3-alternative conformation, demonstrating the importance of the side chains in maintaining the cone conformation. In

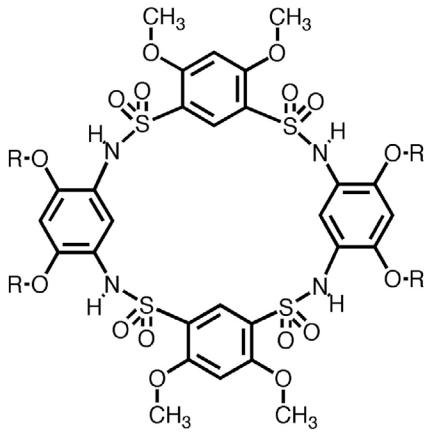

1a: R = n-C_3H_7
1b: R = n-C_5H_{11}

Structure 1.

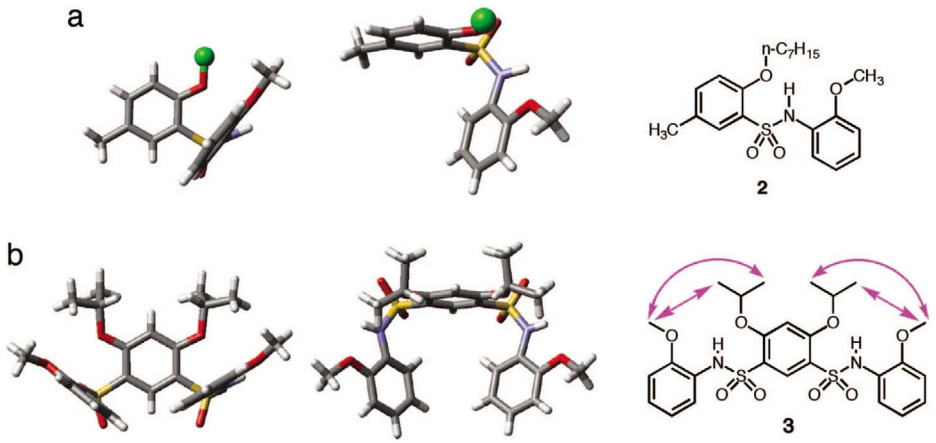

Figure 1. Side and top views of the crystal structure of **2** (*a*) and **3** (*b*). The side-chain ROEs (arrows) revealed by ROE spectroscopy (2 mM in $CDCl_3$, 500 MHz, 295 K; mixing time: 0.3 s) spectrum of **3**. For clarity, the heptyl group of **2** is replaced with a dummy atom.

addition, solid-state structures indicate that these macrocycles, regardless of their cavity sizes, form nanotubular assemblies with pore diameters that are defined by the cavity sizes of the constituent molecules.

Results and Discussion

To probe the origin and possible generality of the stable cone conformations adopted by **1a-b**, noncyclic aromatic sulfonamide **2** and disulfonamide **3**, which can be regarded as fragments of **1a** or **1b**, were investigated by x-ray crystallography and 2D ^{1}H NMR.

The crystal structure of **2** (Fig. 1*a*) reveals a conformation involving two adjacent benzene rings with their planes being nearly perpendicular to each other. This conformation is very similar to that of the diarylsulfonamide motif in the crystal structure of **1a**. The crystal structure of **3** (Fig. 1*b*) reveals a partial cone conformation that is similar to that of **1a**. Similar to **2**, the adjacent benzene rings of **3** are nearly perpendicular to each other, leading to a partially enclosed cavity that is defined by the aromatic rings from the three residues. 2D NMR [rotating-frame Overhauser effect (ROE) spectroscopy] studies of **3** revealed ROEs between the protons of the methoxy and *n*-butyl side chains (see structure in Fig. 1*b*, indicated by arrows) (see Figs. 8–10, in the appendix to this edition). These ROEs are consistent with a solution conformation in which all of the benzene rings and their side chains point to the same side. That no ROEs corresponding to other alternative conformations were detected suggests that the solution conformation of **3** is consistent to that revealed by its crystal structure.

These results clearly demonstrate that the cone conformations adopted by **1a-b** are not due to the cyclization of the oligosulfonamide backbones. Instead, the diarylsulfonamide moiety, with its conformation involving nearly perpendicular adjacent aromatic rings, is solely responsible for the formation of the four-residue macrocycles and their observed shapes. Thus, noncyclic precursors for **1a** or **1b** must have adopted a convergent conformation that facilitated the final cyclization step.

If the diarylsulfonamide moiety is indeed a convergent structural motif, aromatic oligosulfonamide macrocycles with similar conformations, but larger cavities than those of **1a** and **1b**, should be available by including large aromatic rings into the design (see Scheme 1). To probe this possibility, naphthalenedisulfonyl chloride **4** was added to diamines **5a** and **5b** in methylene chloride in the presence of triethylamine, followed by refluxing the solution for 12 h. Indeed, MALDI-TOF indicated that **6a-b** formed as the major product from these one-step reactions. After removal of solvent, the remaining residues were washed with a small amount of methylene chloride, followed by washing with water and acetone and, in the case of **6a**, tetrahydrofuran (THF), and then recrystallized from pyridine–methanol, which led to the isolation of pure **6a** or **6b** as a white solid.

Single crystals of **6a** were grown by slow cooling from pyridine. As Fig. 2 shows, in the solid state, macrocycle **6a** adopts a cone conformation. This conformation has a rough C2 symmetry and a cavity surrounded by the four aromatic residues. The neighboring benzene and naphthalene rings are nearly perpendicular to each other. A dihedral angle of ≈100° exists between the two naphthalene rings, while the two benzene rings of the diamine residue slightly tilt toward the C2 axis. The ether side chains are attached to the wider rim with the sulfonamide oxygens defining the narrower rim. The four N–H groups of **6a** point away from the center of the cavity and are not intramolecularly H-bonded with the two flanking ether oxygens (average NH...O distances of 2.73 and 2.90 Å).

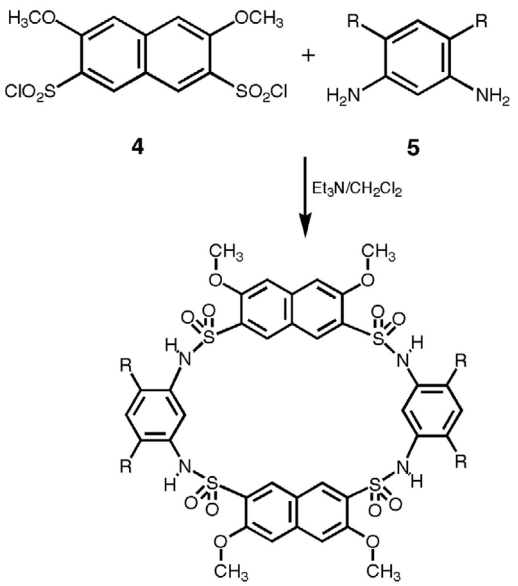

6a: R = -O-*i*-C_5H_{11}; **6b**: R = -O-*n*-C_7H_{15}; **6c**: R = H

Scheme 1.

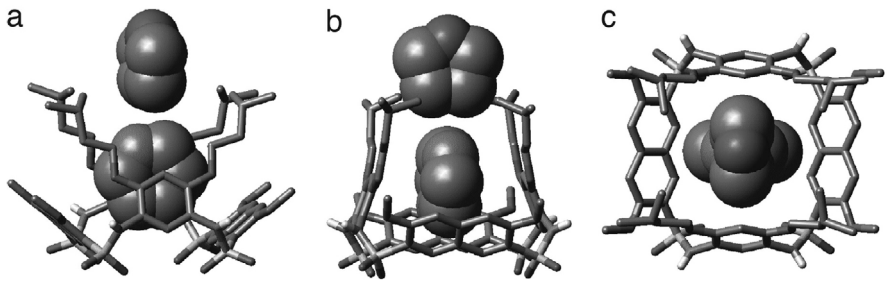

Figure 2. The crystal structure of **6a** shown in side (*a* and *b*) and top (*c*) views. The pyridine and THF molecules are shown in space-filling model. Except for the amide hydrogens, all other hydrogens are removed for clarity. The THF molecule was from the purification step.

As expected, incorporating naphthalene residue into **6a** leads to a cavity (8.47 × 8.89 Å, measured by distances between the centers of nonadjacent aromatic rings) that is larger than that of **1a** (6.98 × 7.97 Å). In contrast to the cavity of **1a**, which could only accommodate small solvent molecules such as DMF, a pyridine molecule is found in the cavity of **6a**. The pyridine molecule is sandwiched between the two benzene rings of the diamine residues, with its plane being perpendicular to those of the naphthalene rings. The benzene rings tilt slightly inward to achieve optimum contact distances (≈3.6 Å) with the pyridine ring (Fig. 2 *b* and *c*). This observation suggests that this class of macrocycles have a sufficiently large, well defined cavity with the potential ability to undergo conformational fine-tuning for binding organic molecules. Even more interesting is the presence of a THF molecule that is "holding up" by the four isopentyl side chains. The THF molecules interact with the host molecule via van der Waals contacts between its methylene groups and the methyl groups on the isopentyl side chains. This result suggests the possibility of designing sophisticated hosts by incorporating different side chains into the macrocycle.

NOESY experiment was carried out with the more soluble **6b**. Nuclear Overhauser effects (NOEs) between the protons of the methoxy and the *n*-heptyl groups were observed (Fig. 3) (see Figs. 11 and 12, in the appendix to this edition), suggesting that the solution conformation of **6b** is indeed similar to that revealed by the solid-state structure of **6a**.

Variable-temperature ^{1}H NMR experiments were performed on **6b** to probe the dynamics of its solution conformation. In deuterated *N*,*N*-dimethylformamide (DMF-d_7), the diastereotopic α- and β-methylene protons of the heptyl side chains appear at ≈3.7 and ≈1.5 ppm at room temperature. Upon lowering temperature, each of these two groups of signals first started to broaden and then split into two separate signals

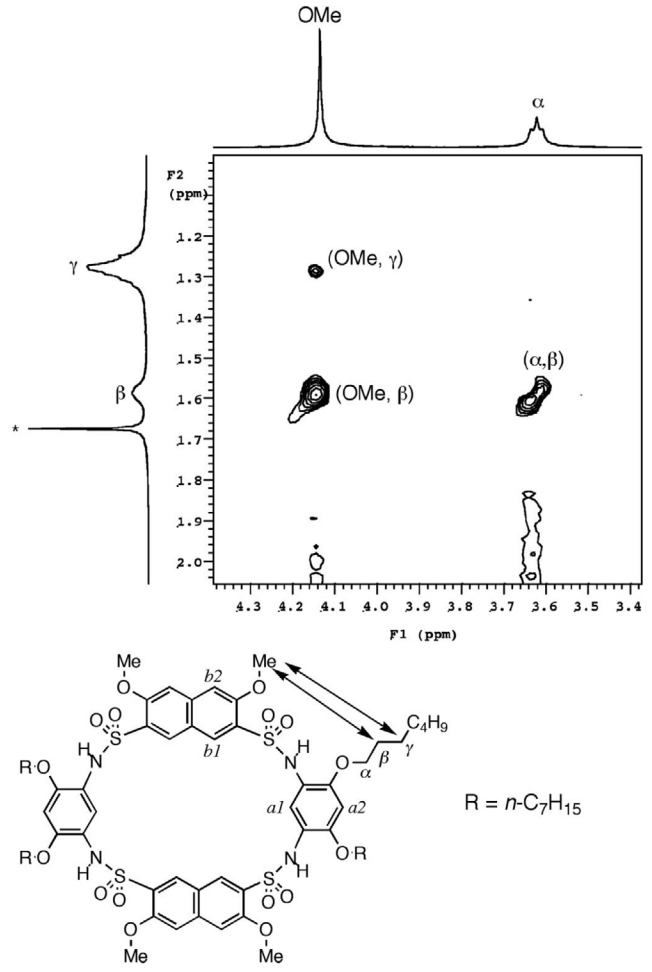

Figure 3. Partial NOESY spectrum of **6b** in $CDCl_3$ at 273 K (500 MHz, 2 mM; mixing time: 0.35 s).

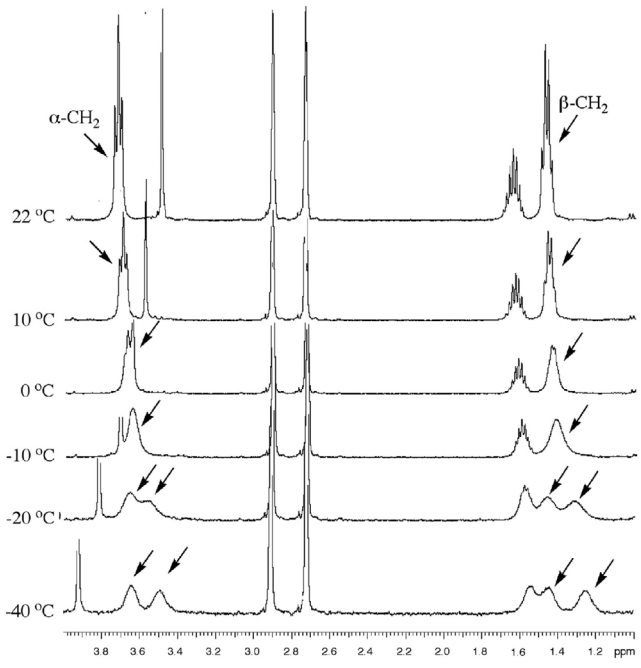

Figure 4. Partial ^{1}H NMR spectra of **6b** in DMF-d_7 (2 mM, 500 MHz) at different temperatures. The signals of the α- and β-methylene protons are indicated by arrows.

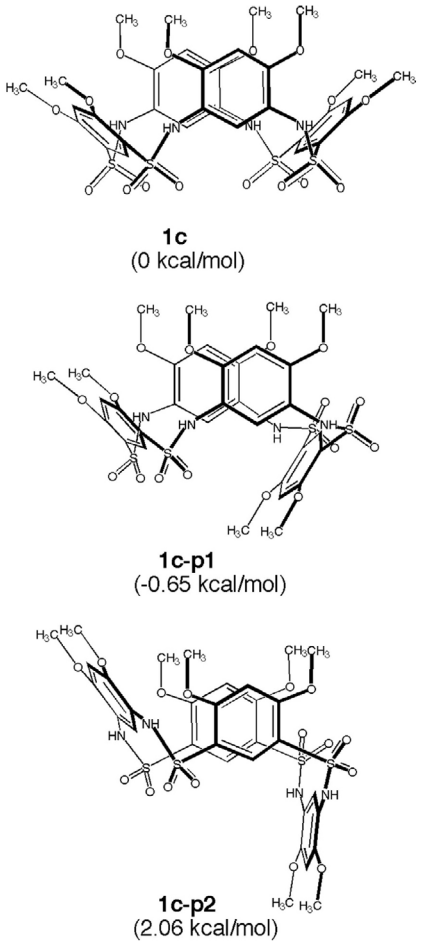

Figure 5. The relative energies of the cone conformation **1c** and its corresponding partial cone conformations **1c-p1** and **1c-p2** based on *ab initio* calculation at the B3LYP/6-311G(d,p) level.

between –10°C and –20°C (Fig. 4). In chloroform-*d* (see Fig. 13, in the appendix to this edition), the α- and β-methylene protons of **6b** similarly split into two signals but at much lower temperatures (below –35°C). In both solvents, no other ^{1}H signals showed any splitting within the temperature ranges examined. These results indicate that, at room temperature, the observed signals for the α- and β-methylene protons were the result of rapid interconversion of the cone conformations, in a way similar to the ring-flipping of cyclohexane. The low coalescence temperatures suggest that the energy barrier for the interconversion of the cone conformations is very small. The solvent-dependence of the coalescence temperature is probably due to stabilization of the cone conformation by differential guest binding (DMF vs. chloroform) or by enhanced intermolecular interaction between the macrocycles.

The interconversion of two cone conformations requires the inversion of the aromatic walls of the system, which should go through partial cone conformations. To investigate the stability of the cone and partial cone conformations, *ab initio* calculation was performed on cyclic tetrasulfonamide **1c**, an analog of **1a** and **1b**. In addition to the cone conformation, two partial cone conformations, **1c-p1** and **1c-p2**, are the possible intermediates for the interconversion of the cone conformations of **1c**. The partial cone conformations **1c-p1** and **1c-p2** are created by inverting one of the benzenedisulfonyl residues or one of the benzenediamine residues (Fig. 5). Results from the *ab initio* study revealed that the stabilities of cone conformation **1c** and one of the partial cone conformations, **1c-p1**, are nearly the same, whereas a difference of 2.06 kcal/mol, was revealed between **1c** and the other partial cone conformation, **1c-p2**. These results suggest that the interconversion of the cone conformations can readily happen by going through the partial cone conformations, most likely via **1c-p1**.

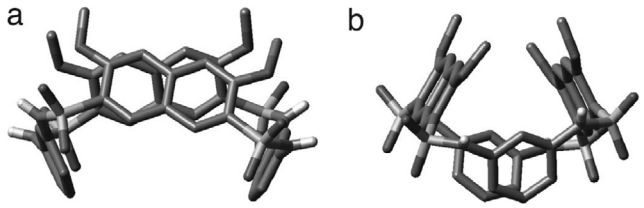

Figure 6. The crystal structure of macrocycle **6c** viewed from the side of one of the two naphthalene residues (*a*) and from the side of one of the two benzene residues (*b*).

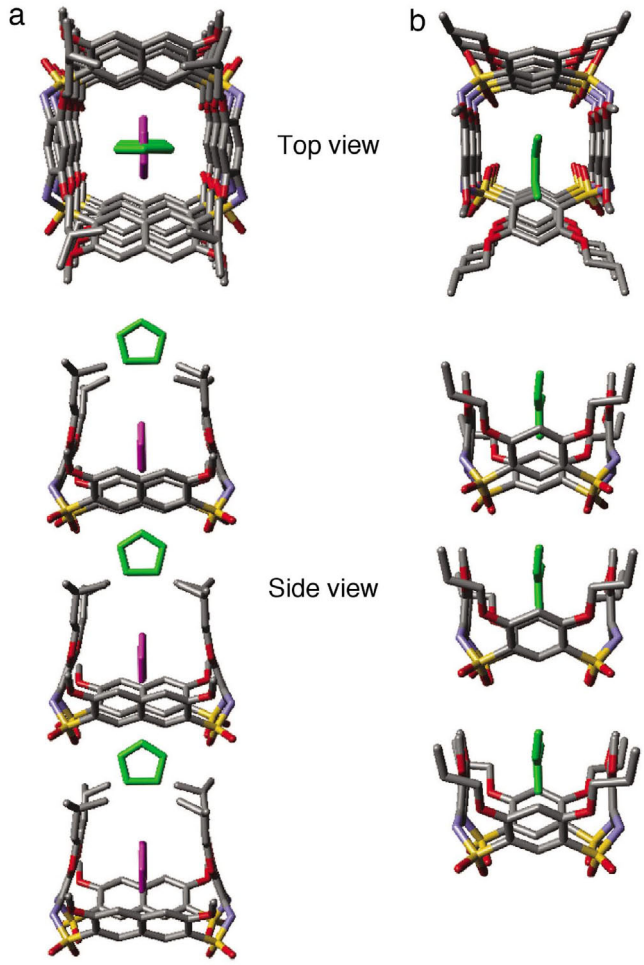

Figure 7. Top and side views of the solid-state tubular assemblies of **6a** (*a*) and **1a** (*b*). (*a*) Three molecules of **6a** are shown. The solvent molecules (pyridine, purple; THF, green) in the macrocyclic cavity are also shown. (*b*) Three molecules of **1a** are shown. The solvent molecules (DMF, green) in the cavity are also shown. For clarity, all H atoms are removed.

To probe the role of the alkoxy side chains on maintaining the cone conformations of this class of molecules, compound **6c** was prepared by treating 1,3-phenylenediamine with naphthalenedisulfonyl chloride **4**. Macrocycle **6c** can be regarded as being derived from removing the alkoxy side chains on the diamino benzene residues of **6a-b**. X-ray quality crystals of **6c** were obtained from a solvent mixture containing DMSO:EtOH:THF (10:0.5:0.5) by slow cooling. The crystal structure of **6c** is shown in Fig. 6. Similar to macrocycles **1** and **6a-b**, the adjacent aromatic rings of **6c** are nearly perpendicular to each other. However, in contrast to the cone conformations observed for the other tetrasulfonamide macrocycles, the solid-state structure of **6c** involves the inversion of the benzene rings, leading to a conformation reminiscent of the 1,3-alternate conformation of calix[4]arenas (Fig. 6; see also Fig. 14, in the appendix to this edition). Such a conformation of **6c** demonstrates the critical role of the alkoxy side chains in maintaining the cone conformations of macrocycles **1** and **6a-b**. We believe that the repulsive interaction between the ether and sulfonamide oxygens are responsible for maintaining the observed cone conformation of macrocycles **1** and **6a-b**.

Finally, examining the solid-state structures of macrocycles **6a** and **1a** indicated tubular assemblies consisting of molecules stacked above one another (Fig. 7). In each case, the pore size of the porous column is defined by the cavity size of the macrocyclic molecules. For both **6a** and **1a**, solvent molecules are observed in the macrocyclic cavities. The 2D NMR and x-ray results imply that, both in solution and in the solid state, tubular assembly may be a general phenomenon associated with these tetrasulfonamide macrocycles. More detailed studies could lead to the creation of nanotubular structures with a variety of pore sizes based on this predictable assembling pattern.

Conclusion

In summary, we have demonstrated that the diarylsulfonamide moiety with flanking alkoxy groups is a reliable structural motif for designing cone-shaped macrocyclic aromatic tetrasulfonamides. This motif adopts a well defined conformation with a 90° dihedral angle, based on which macrocyclic aromatic tetrasulfonamides with stable cone conformations containing cavities of various sizes are formed in one step. The diameter of a cavity is determined by the size of the incorporated aromatic rings. Guest molecules can fit into the cavity of a macrocycle with the proper size. The tubular assemblies of both **1a** and **6a** in the solid state, and very likely in solution, suggest an exciting possibility of developing a general system that allows the design of nanotubular structures with predictable assembly and tunable pore sizes. Thus, these readily available, cone-like macrocycles represent a previously undescribed class of shape-persistent (6, 7), cavity-containing molecules that should serve as useful building blocks for developing various hosts and nanoporous structures.

Materials and Methods

NMR analyses were carried out on Varian INOVA 500 spectrometer (500 MHz) in $CDCl_3$ or DMF-d_7. Tetramethylsilane (TMS) was used as the internal standard for ^1H NMR and ^{13}C NMR. Chemical shifts are reported in ppm values downfield from TMS, and *J* values are reported in Hz.

Compound 2. ^1H NMR (500 MHz, $CDCl_3$) δ: 7.67 (s, 1H), 7.55 (s, 1H), 7.51 (d, J = 8.0 Hz, 1H), 7.21 (d, J = 8.2 Hz, 1H), 6.96 (t, J = 7.7 Hz, 1H), 6.86~6.74 (m, 3H), 4.04 (t, J = 6.7 Hz, 2H), 3.74 (s, 3H), 2.26 (s, 3H), 1.91 (m, 2H), 1.53 (m, 2H), 1.40~1.30 (m, 6H), 0.90 (t, J = 6.18 Hz, 3H). MS (MALDI-TOF), Calcd for $C_{21}H_{29}NO_4S$ 391.18 (M^+), found 414.1 ($M+Na^+$). ^{13}C NMR (100.6 MHz, $CDCl_3$) δ: 154.04, 148.86, 135.05, 130.84, 129.52, 126.73, 126.61, 124.16, 121.11, 119.67, 112.58, 110.50, 69.25, 55.65, 31.73, 29.16, 25.89, 22.63, 20.27, 14.08.

Compound 3. Compund **3** was prepared by treating the corresponding benzenedisulfonyl chloride (0.5 mmol) with *o*-anisidine (0.11 ml, 1 mmol) in CH_2Cl_2 in the presence of triethylamine. Yield: 70%, colorless crystal, mp: 174–176°C. ^1H NMR (500 MHz, $CDCl_3$) *δ*: 8.51 (s, 1H), 7.40 (d, J = 8.0 Hz, 2H), 7.38 (s, 2H), 6.96 (t, J = 7.8 Hz, 2H), 6.82 (t, J = 7.5 Hz, 2H), 6.76 (d, J = 8.0 Hz, 2H), 6.32 (s, 1H), 4.62 (m, 2H), 3.78 (s, 6H), 1.39 (d, 12H). MS (MALDI-TOF), Calcd for $C_{26}H_{32}N_2O_8S_2$ 564.16 (M^+), found 587.1 ($M+Na^+$). ^{13}C NMR (100.6 MHz, $CDCl_3$) *δ*: 160.11, 147.95, 134.82, 126.32, 123.93, 121.44, 118.84, 118.00, 110.47, 98.63, 72.65, 55.59, 21.48; MS (ESI) *m/z*, Calcd for $C_{24}H_{39}NO_6$ 437.28 (M^+), found 438.3 ($M+H^+$).

2,7-Dimethoxynaphalene-3,6-Disulfonyl Chlorides (4). The following procedure for preparation of **4** was based on a similar method reported in ref. 24. The commercially available disodium 2,7-dihydroxynaphalene-3,6-disulfonate (**4a**; technical, 5 g, 13.7 mmol) and NaOH (2.2 g, 55 mmol) were dissolved in water (30 ml), and dimethyl sulfate (5.2 ml, 55 mmol) was added dropwise to the solution under stirring. After maintaining the temperature at ≈65°C for 3 h, NaCl (6 g) was added to the mixture to precipitate 2,7-dimethoxynaphalene-3,6-disulfonate (**4b**), which was filtered off, washed with saturated NaCl, and dried. Repeating the above steps often can lead to the isolation a small amount of **4b** from the filtrate. Half of the obtained **4b** (3.14 g) was suspended in dry DMF (5 ml), and thionyl chloride (1.5 ml, 20 mmol) was added dropwise under stirring, along with the other half of the methoxy salt in portions, while the temperature was kept at <15°C. After the mixture was stirred for another 3 h at room temperature, ice and water were added, and the product was removed by filtration, washed with ice-water, and dried in a desiccator. Recrystallization of the crude product from $CHCl_3$–CH_3OH gave 2,7-dimethoxynaphalene-3,6-disulfonyl chlorides (**4**) (1.27 g, 24%), mp 240–242°C.

General Procedures for Preparing 6a–c. 4,6-Dialkoxy-1, 3-diaminobenzene (**3**) (1.1 mmol) was dissolved in CH_2Cl_2 (15 ml) to give solution A. Disulfonyl chlorides **4** (0.385 g, 1 mmol) was dissolved in CH_2Cl_2 (15 ml) to give solution B. Solutions A and B and triethylamine (0.28 ml, 2 mmol) were added simultaneously to a flask at room temperature, followed by heating the reaction mixture under reflux for 12–24 h. After removing the solvent, the crude product was washed with a small amount of methylene chloride, water, and acetone. The product was then recrystallized with pyridine–methanol to give **6a** or **6b** as white solids. The yields have not been optimized.

Compound 6a: Yield: 30%. ^1H NMR (500 MHz, 273K, DMF-d_7) δ: 7.99 (s, 4H), 7.75 (s, 4H), 7.19 (s, 2H), 7.09 (s, 4H), 5.97 (s, 2H), 4.14 (s, 12H), 3.62 (t, J = 6.2 Hz, 8H), 1.59 (m, 8H), 1.27 (m, 32H), 0.90 (t, J = 7.0, 12H). MS (MALDI-TOF), Calcd $C_{65}H_{92}N_4O_{16}S_4$, 1312.54 (M^+), found 1335.53 ($M+Na^+$).

Compound 6b: Yield: 20%. ^1H NMR (500 MHz, 273K, DMF-d_7) δ: 7.99 (s, 4H), 7.75 (s, 4H), 7.19 (s, 2H), 7.09 (s, 4H), 5.97 (s, 2H), 4.14 (s, 12H), 3.62 (t, J = 6.2 Hz, 8H), 1.59 (m, 8H), 1.27 (m, 32H), 0.90 (t, J = 7.0, 12H). MS (MALDI-TOF), Calcd $C_{65}H_{92}N_4O_{16}S_4$, 1312.54 (M^+), found 1335.53 ($M+Na^+$).

Compound 6c: Yield: 28%. ^1H NMR (500 MHz, 273K, DMSO) δ: 8.57 (s, 4H), 8.03 (s, 4H), 7.43 (s, 2H), 7.40 (d, J = 7.5 Hz, 4H), 7.01 (s, 2H), 6.95 (t, J = 7.9 Hz, 2H), 6.79 (s, 2H), 4.09 (s, 12H). MS (MALDI-TOF), Calcd $C_{36}H_{32}N_4O_{12}S_4$, 840.6 (M^+), found 863.5 ($M+Na^+$), 879.4 ($M+K^+$).

X-Ray Data. Compounds **2** and **3** were crystallized from DMF by slow cooling. Compound **2**: space group P-1, a = 8.5122 (12) Å, b = 8.8900 (12) Å, c = 14.309 (2) Å, α= 84.448 (2)°, β= 88.069 (2)°, γ= 75.994 (2)°. Compound **3**: space group $P2_12_12_1$, a = 9.0348 (7) Å, b = 12.8363 (9) Å, c = 24.4291 (18) Å. Compound **6a** was crystallized from pyridine by slow cooling: space group C2/c, a = 32.659 (7) Å, b = 11.398 (2) Å, c = 26.898 (6), β= 103.535 (3)°. Compound **6c** was crystallized from a solvent mixture containing DMSO:EtOH:THF (10:0.5:0.5) by slow cooling: space group C2/c, a = 31.333 (6) Å, b = 14.016 (3) Å, c = 14.718 (3) Å, β= 99.59 (3)°.

***Ab Initio* Calculations.** The *ab initio* calculations were carried out by using the GAUSSIAN 03 package (Revision C.02; ref. 25). The geometry of each conformer was optimized at the B3LYP/6-311G(d,p) level of theory. The frequencies and zero-point energies were also calculated at the B3LYP/6-311G(d) level of theory. No imaginary frequencies were found for the conformers. The total-energy calculations (including the zero-point energy corrections) indicate that the partially flipped conformer **1c-p1** is slightly lower in energy (by 0.65 kcal/mol) than the fully flipped conformer **1c**.

Acknowledgements

This work was supported by the TransCentury Training Program Foundation for the Talents, Ministry of Education of China, National Natural Science Foundation of China Grant 20372010 (to L.H.), the Changjiang Scholar Program (to B.G.), National Science Foundation Grant CHE-0314577 (to B.G. and X.C.Z.), and Office of Naval Research Grant N000140210519 (to B.G.).

Abbreviations: DMF, *N*,*N*′-dimethylformamide; DMF-d_7, deuterated *N*,*N*-dimethylformamide; ROE, rotating-frame Overhauser effect; THF, tetrahydrofuran.

Author contributions: L.H. and B.G. designed research; L.H., Y.A., L.Y., W.F., M.L., D.Z., K.Y., C.Z., X.C.Z., and B.G. performed research; L.H., Y.A., L.Y., M.L., K.Y., C.Z., X.C.Z., and B.G. analyzed data; and B.G. wrote the paper.

The atomic coordinates have been deposited in the Cambridge Structural Database, Cambridge Crystallographic Data Centre, Cambridge CB2 1EZ, United Kingdom (CSD reference nos. CCDC-288116, -288117, -288118, and -297380).

References

1. Purse, B. W. & Rebek, J. (2005) *Proc. Natl. Acad. Sci. USA* **102**, 10777–10782.
2. Vriezema, D. M., Aragones, M. C., Elemans, J. A. A. W., Cornelissen, J. J. L. M., Rowan, A. E. & Nolte, R. J. M. (2005) *Chem. Rev.* **105**, 1445–1489.
3. Hoger, S. (2005) *Angew. Chem. Int. Ed.* **44**, 3806–3808.
4. Zhao, D. H. & Moore, J. S. (2003) *Chem. Commun.* 807–818.
5. Böhmer, V. (1995) *Angew. Chem. Int. Ed.* **34**, 713–745.
6. Ikeda, A. & Shinkai, S. (1997) *Chem. Rev.* **97**, 1713–1734.
7. Rebek, J. (2000) *Chem. Commun.* 637–643.
8. Arduini, A., Pochini, A., Secchi, A. & Ugozzoli, F. (2001) in *Calixarenes* eds. Asfari, Z., Böhmer, V., Harrowfield, J.& Vicens, J. (Kluwer Academic, Dordrecht, The Netherlands), pp. 457–475.
9. Thondorf, I. (2001) in *Calixarenes* eds. Asfari, Z., Böhmer, V., Harrowfield, J.& Vicens, J. (Kluwer Academic, Dordrecht, The Netherlands), pp. 280–295.
10. Dalla Cort, A. & Mandolini, L. (2000) in *Calixarenes in Action* eds. Mandolini, L. & Ungaro, R. (Imperial College Press, London), pp. 85–110.
11. Shinkai, S., Fujimoto, K., Otsuka, T. & Ammon, H. L. (1992) *J. Org. Chem.* **57**, 1516–1523.
12. Wang, D. F. & Wu, Y. D. (2004) *J. Theor. Comput. Chem.* **3**, 51–68.
13. Wenz, G., Han, B. H. & Muller, A. (2006) *Chem. Rev.* **106**, 782–817.
14. Georghiou, P. E., Li, Z. P., Ashram, M., Chowdhury, S., Mizyed, S., Tran, A. H., Al-Saraierh, H. & Miller, D. O. (2005) *Synlett* 879–891.
15. Arduini, A., McGregor, W. M., Pochini, A., Secchi, A., Ugozzoli, F. & Ungaro, R. (1996) *J. Org. Chem.* **61**, 6881–6887.
16. van Hoorn, W. P., Morshuis, M. G. H., van Veggel, F. C. J. M. & Reinhoudt, D. N. (1998) *J. Phys. Chem. A* **102**, 1130–1138.
17. Kusano, T., Tabatabai, M., Okamoto, Y. & Böhmer, V. (1999) *J. Am. Chem. Soc.* **121**, 3789–3790.
18. Vysotsky, M. O., Mogck, O., Rudzevich, Y., Shivanyuk, A., Böhmer, V., Brody, M. S., Cho, Y. L., Rudkevich, D. M. & Rebek, J. (2004) *J. Org. Chem.* **69**, 6115–6120.
19. Rudzevich, Y., Vysotsky, M. O., Böhmer, V., Brody, M. S., Rebek, J., Broda, F. & Thondorf, I. (2004) *Org. Biomol. Chem.* **2**, 3080–3084.
20. Hooley, R. J. & Rebek, J. (2005) *J. Am. Chem. Soc.* **127**, 11904–11905.
21. Gong, B. (2000) *Chem. Eur. J.* **7**, 4336–4342.
22. Sanford, A. R. & Gong, B. (2003) *Curr. Org. Chem.* **7**, 1649–1659.
23. He, L., An, Y., Yuan, L. H., Yamato, K., Feng, W., Gerlitz, O., Zheng, C. & Gong, B. (2005) *Chem. Commun.* 3788–3790.
24. Bosshard, H. H., Mory, R., Schmid, M. & Zollinger, H. (1959) *Helv. Chim. Acta* **42**, 1653–1658.
25. Frisch, M. J., Trucks, G. W., Schlegel, H. B., Scuseria, G. E., Robb, M. A., Cheeseman, J. R., Montgomery, J. A. Jr, Vreven, T., Kudin, K. N. & Burant, J. C., *et al.* (2003) *GAUSSIAN 03* (Gaussian, Pittsburgh), Revision C. 02.

Appendix: Supporting Information (following pages)

Figure 8. ^{1}H NMR spectrum of compound **3** in $CDCl_3$.

Figure 9. Partial ROESY spectrum of **3**in $CDCl_3$.

Figure 10. ^{13}C NMR spectrum of compound **3** in $CDCl_3$.

Figure 11. ^{1}H NMR spectrum of compound **6a** in DMF-d_7.

Figure 12. 1D ^{1}H NMR spectrum of compound **6b** in $CDCl_3$.

Figure 13. Variable-temperature 1D ^{1}H NMR spectra of **6b** in $CDCl_3$.

Figure 14. 1D ^{1}H NMR spectrum of compound **6c** in DMSO-d_6.

Fig. 8. ^{1}H NMR spectrum of compound **3** in $CDCl_3$

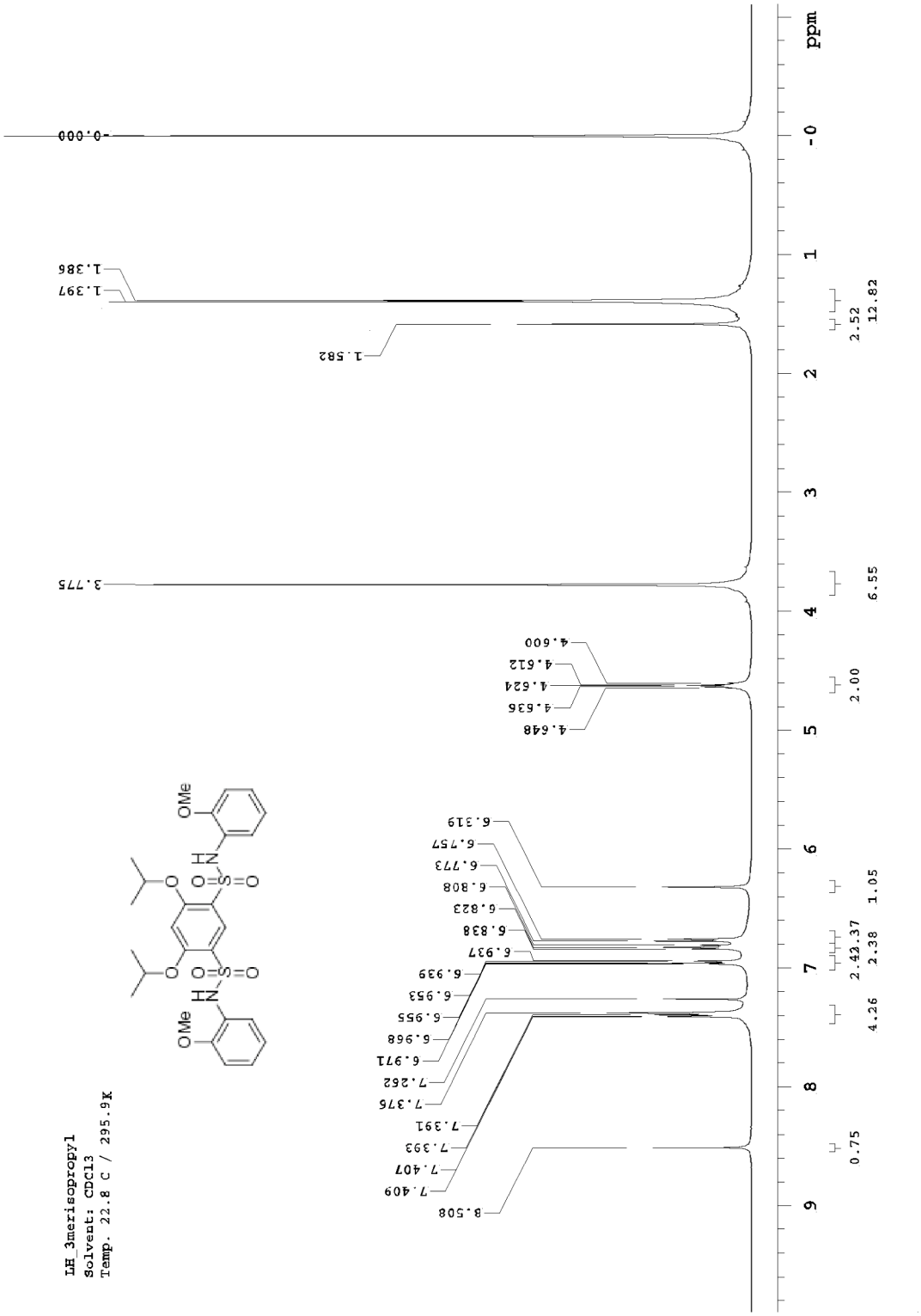

Fig. 9. ^{13}C NMR spectrum of compound **3** in $CDCl_3$

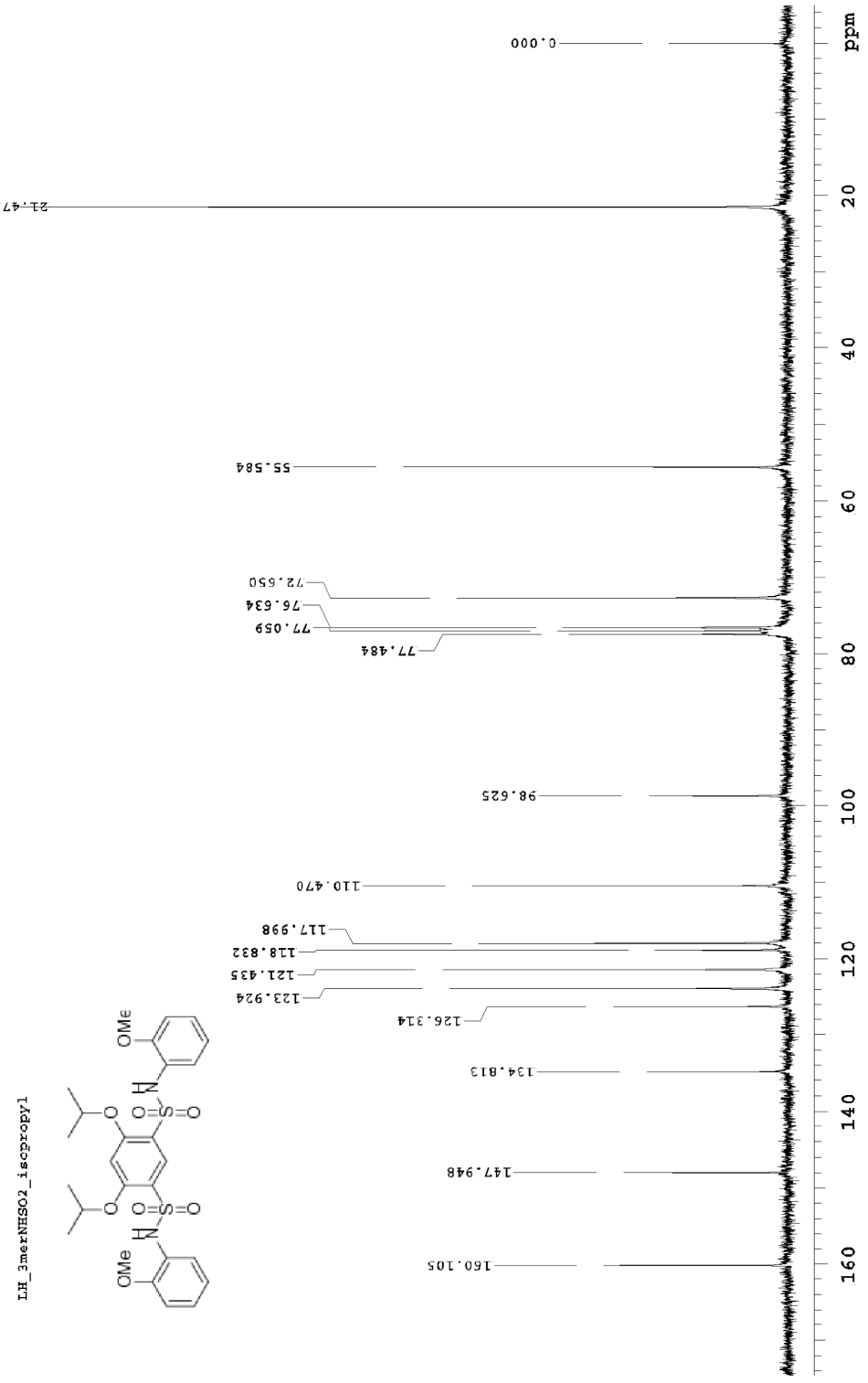

Fig. 10. Partial ROESY spectrum of **3** (2 mM) showing the contacts between OMe and side chains protons in $CDCl_3$ at 295 K (500MHz, mixing time: 0.30 s)

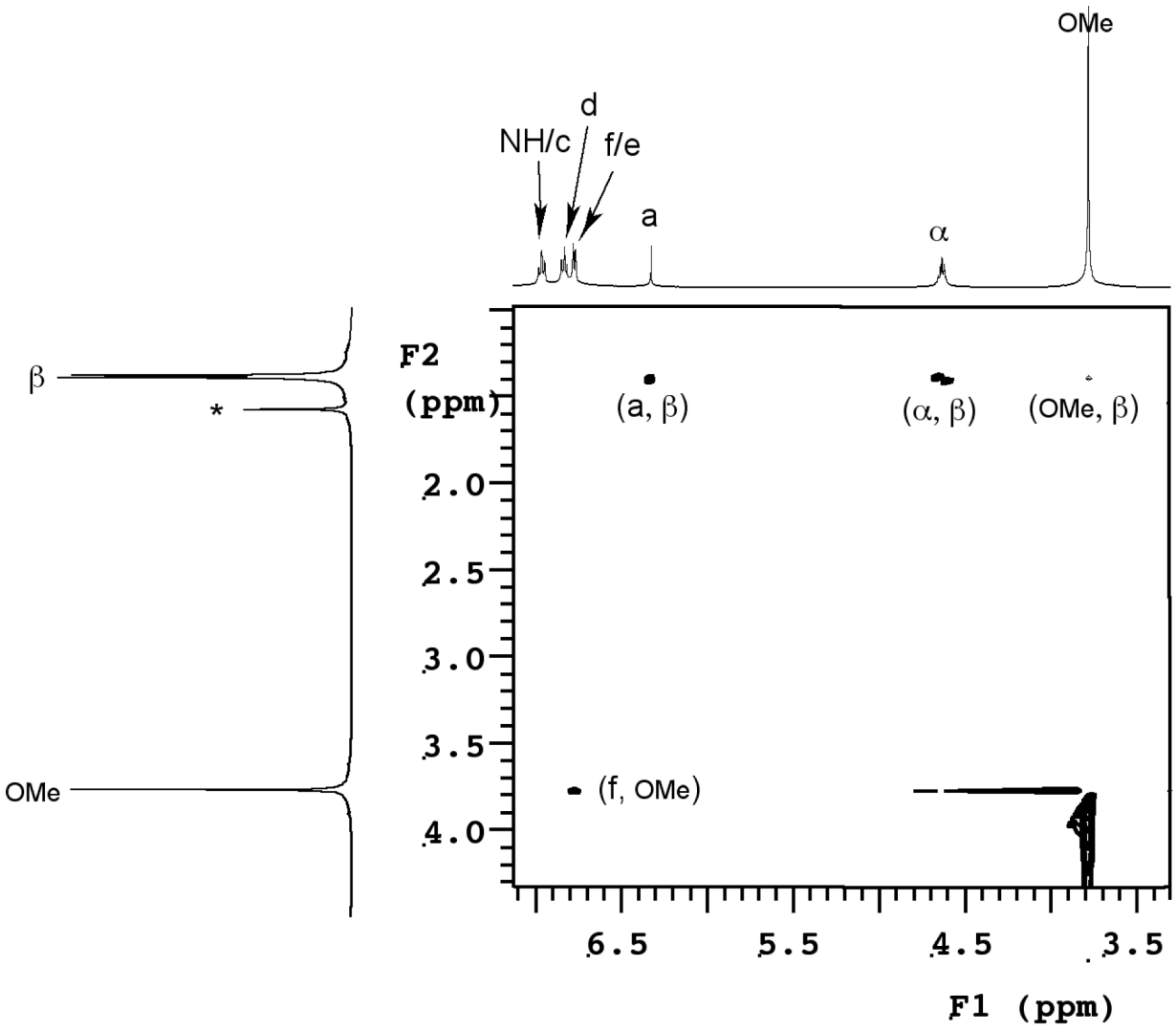

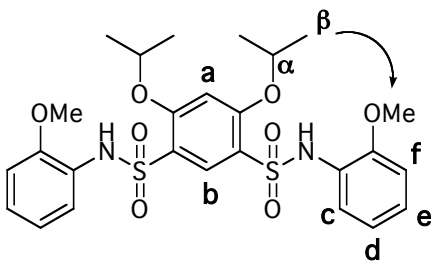

Fig. 11. ^{1}H NMR spectrum of compound **6a** in DMF-d_7

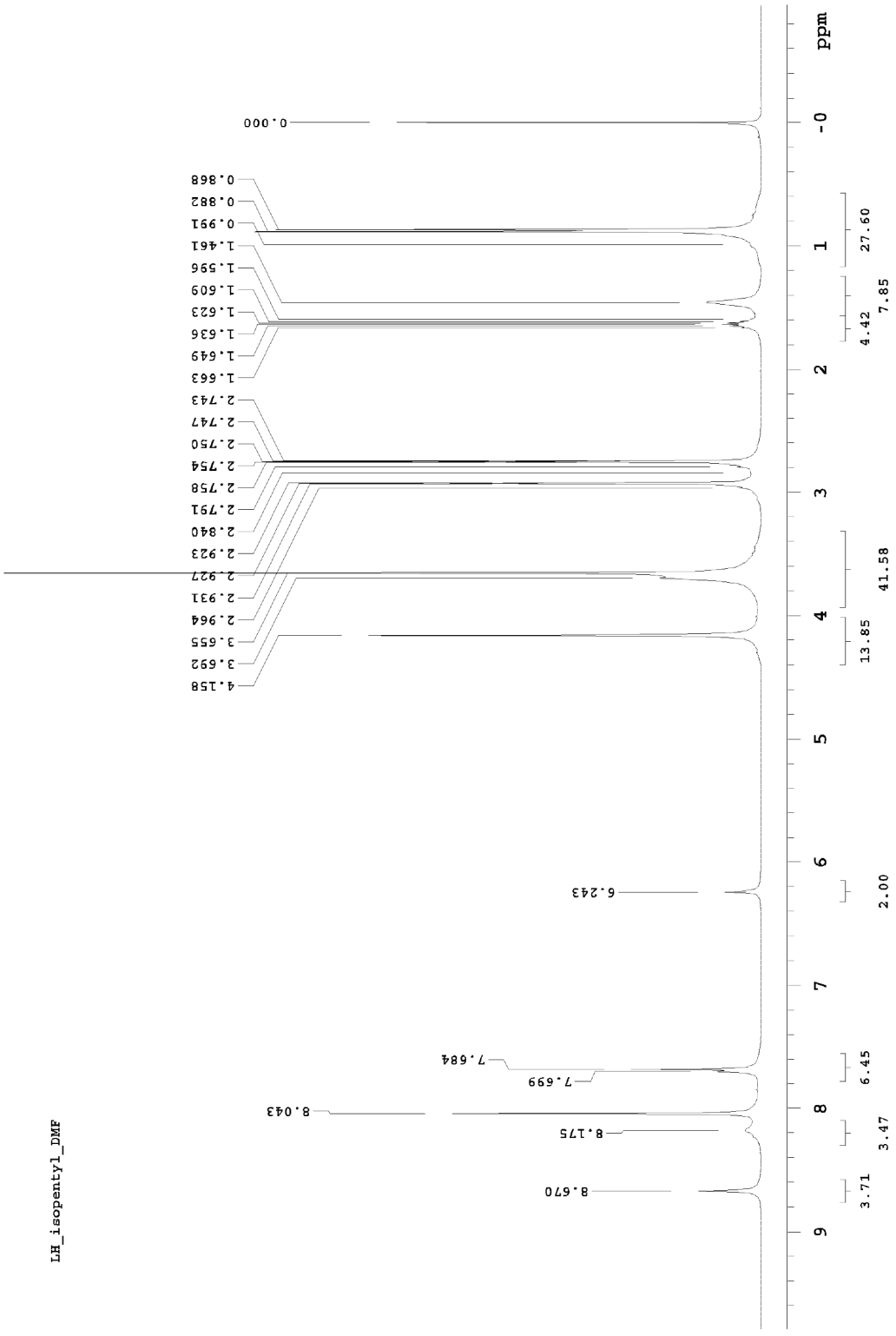

Fig. 12. 1D ^{1}H NMR spectrum of compound **6b** in $CDCl_3$

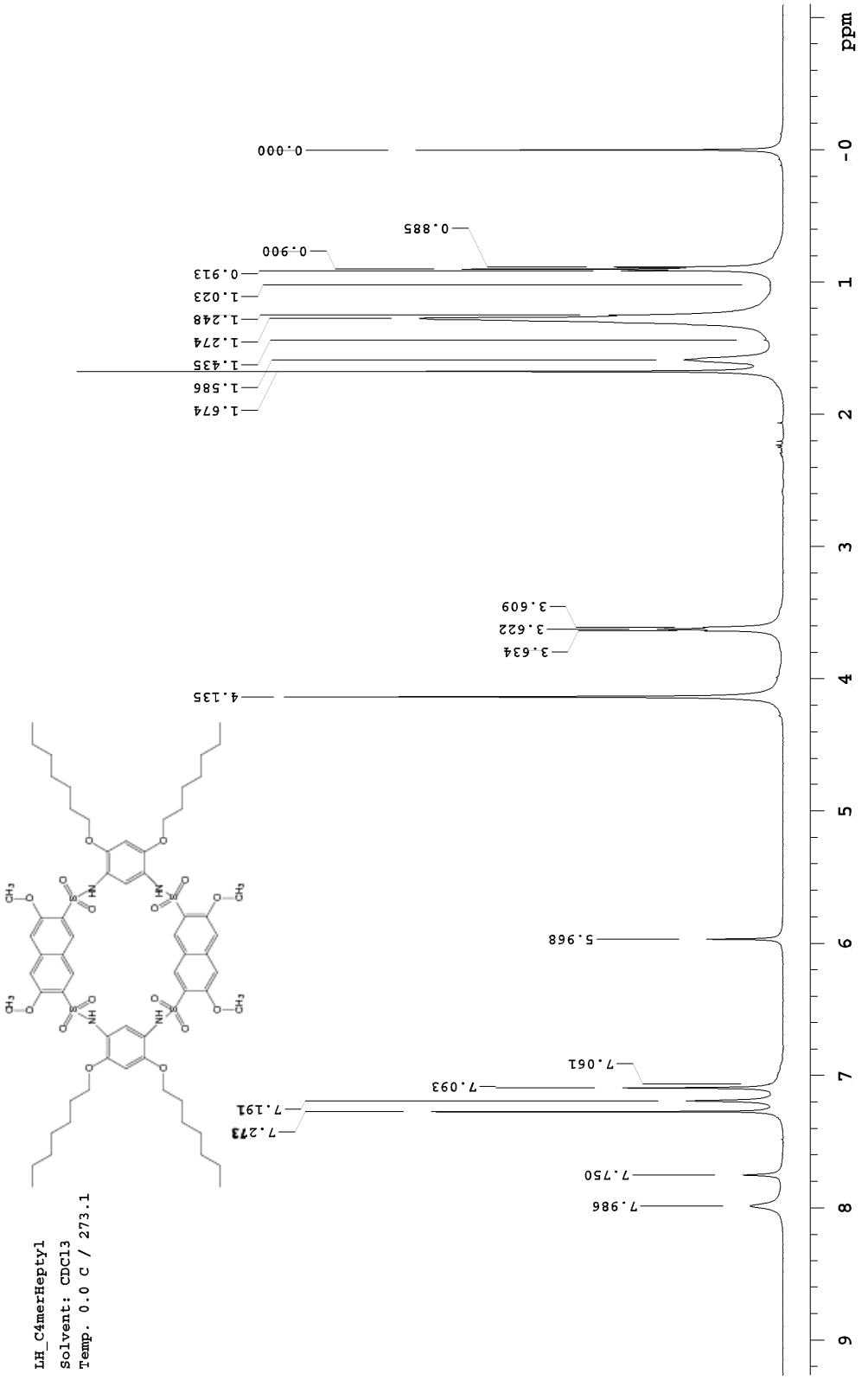

Fig. 13. Variable temperature 1D 1H NMR spectra of **6b** in $CDCl_3$ (2 mM, 500 MHz).

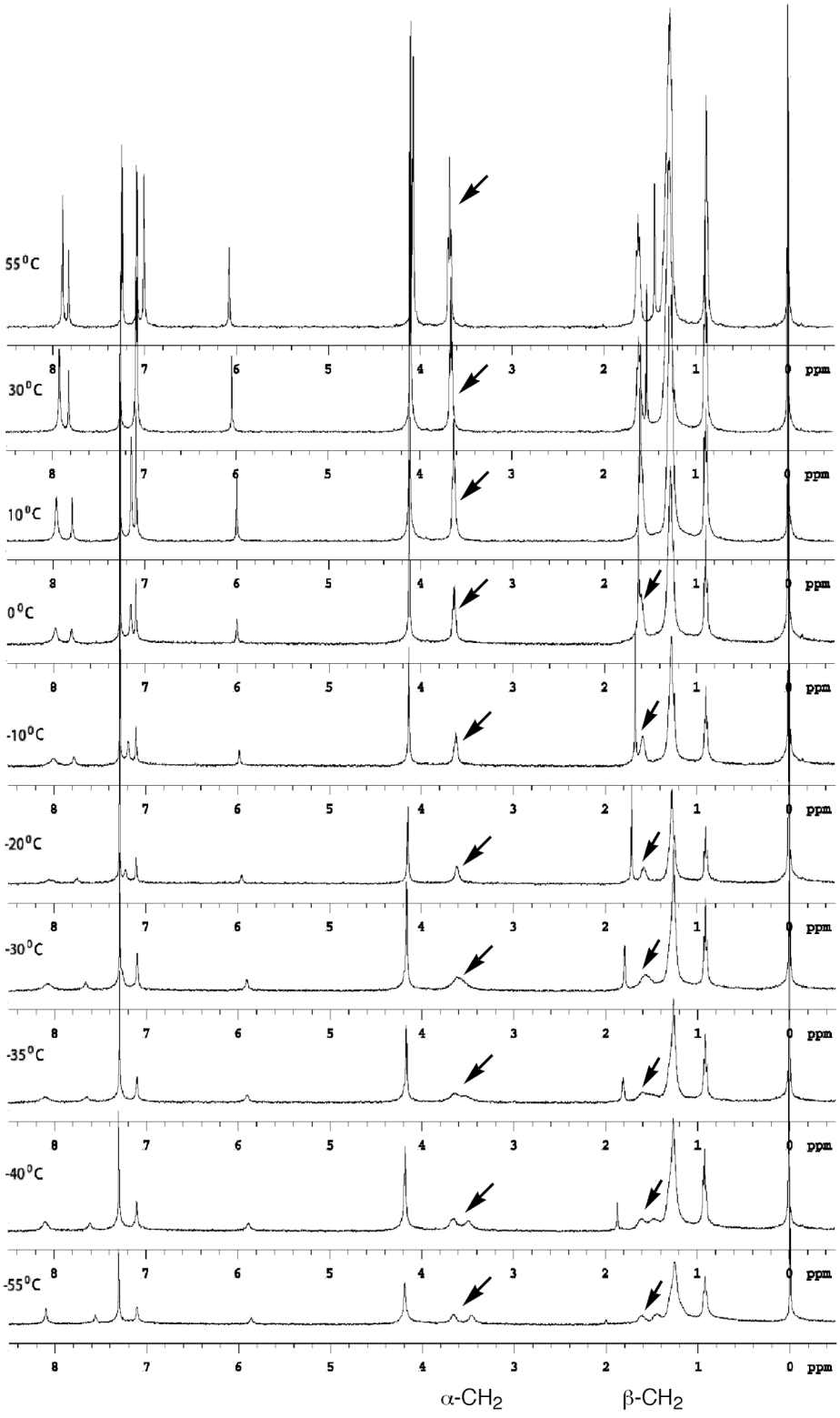

Fig. 14. 1D ^{1}H NMR spectrum of compound **6c** in DMSO-d_6